Beam Index Modulation Wireless Communication with Analog Beamforming

Ding, Y., Fusco, V., Shitvov, A., & Xiao, Y. (2018). Beam Index Modulation Wireless Communication with Analog Beamforming. *IEEE Transactions on Vehicular Technology*, *67*(7), 6340-6354. https://doi.org/10.1109/TVT.2018.2819728

Published in:
IEEE Transactions on Vehicular Technology

Document Version:
Peer reviewed version

Beam Index Modulation Wireless Communication with Analog Beamforming

Yuan Ding, Vincent Fusco, *Fellow*, *IEEE*, Alexey Shitvov, Yue Xiao, *Member*, *IEEE*, and Hailin Li

***Abstract*—In this paper, we propose a new architecture and performance analysis for beam index modulation (BIM) wireless communication implemented with the aid of analog beamforming. The BIM concept is presented in order to extend and adapt the spatial modulation (SM) concept to sparse wireless communication channel environments. It is shown that when compared with the conventional beamforming and SM strategies, the BIM system can achieve higher spectrum efficiency in high signal to noise ratio (SNR) and non-line-of-sight (nLoS) sparse channel scenarios. Furthermore, different to the previous spatial scattering modulation (SSM) work the proposed BIM architectures have reduced hardware complexity, and, importantly, in some nLoS sparse channel conditions the BIM can also outperform the SSM. The above findings were further validated by some demonstrative experiments that were conducted at 10 GHz.**

***Index Terms*—Beam index modulation (BIM), beamforming, spatial modulation (SM), spatial scattering modulation (SSM), spectral efficiency.**

I. Introduction

MULTIPLE-INPUT-MULTIPLE-OUTPUT (MIMO) techniques, [1], which are capable of achieving a multiplexing gain or diversity gain, have been incorporated in modern wireless communications standards, such as IEEE 802.11n, IEEE 802.16e, and 3GPP Long-Term Evolution (LTE).

The emerging technique of spatial modulation (SM) [2]–[4], can be regarded as a hardware-constrained MIMO scheme, where only a single radio frequency (RF) chain is used and which conveys some extra information bits through the indices of activated transmit antennas in an array that are updated in each channel signaling use. This single stream of data in each time slot avoids inter-channel interference that can be severe in multi-stream data transmission systems. In the conventional spatial multiplexing (SMX) MIMO schemes, all transmit and receive antennas are activated in order to create multiple virtual channels for parallel data transmission. Thus, in both transmit and receive sides, multiple RF chains with the numbers equaling those of the associated antennas are required, increasing the complexity, cost, and power consumption of the system. In contrast, the SM system could operate using only a single RF chain, solving the issues associated with the SMX-MIMO mentioned above, though the achievable spectral efficiency is lower than that in the corresponding Vertical Bell Laboratories layers space-time (V-BLAST) system [4]. In other words, the SM technique is able to strike an attractive trade-off among hardware complexity, energy efficiency [5], and achievable transmission rates or spectral efficiency [6]. In the past a few years, it has been shown that this trade-off can be tuned using some SM variants. For example, in order to increase the spectral efficiency in the standard SM systems with slightly sacrificing the hardware complexity and/or energy efficiency, generalized SM (GSM) [7]–[9], multiple-active SM (MA-SM) [10]–[12], quadrature SM (QSM) [13], [14], and enhanced SM (ESM) [15] have been proposed and extensively studied. It is noted that the SM systems can operate effectively only when the wireless propagation channels are multipath-rich such that a unique channel impulse response is associated with each transmit antenna [6], facilitating the detection of transmit antenna indices at receive sides. The assumption of this high-rank channel condition, however, cannot be easily satisfied at higher operation frequencies, as a principal characteristic of such higher frequency wireless channels is their high path loss which limits the number of propagation rays linking transmitters and receivers. One solution was recently proposed in [16]–[18], which modified the line-of-sight (LoS) MIMO [19], [20] to construct SM systems. Apparently, this SM-LoS-MIMO architecture relies on the LoS links, and it was concluded that non-line-of-sight (nLoS) components are harmful and should be avoided [18]. Those channel conditions, generally, can be satisfied in millimeter-wave (mmWave) indoor environment, as nLoS paths typically suffer from much greater loss contributed by reflections and larger path length as compared to the LoS path [21]. However, some inherent characteristics of the SM-LoS-MIMO limit its applications in some important scenarios. For example, *i*) it, like its predecessor LoS-MIMO, is only suitable for fixed wireless access [22], but not mobile applications, as the LoS channels can only be made orthogonal along a boresight link with a fixed length when the antenna element spacings, at both transmit and receive sides, are chosen beforehand, i.e., (25) in [16]; *ii*) since the antenna element spacing is normally much greater than a

The manuscript was submitted on August 28, 2017. This work was supported by the EPSRC (UK) under Grants EP/N020391/1 and EP/P000673/1.

Y. Ding is with the Institute of Sensors, Signals and Systems (ISSS), Heriot-Watt University, Edinburgh, United Kingdom, EH14 4AS (e-mail: yuan.ding@hw.ac.uk).

V. Fusco is with the Institute of Electronics, Communications and Information Technology (ECIT), Queen's University of Belfast, Belfast, United Kingdom, BT3 9DT.

A. Shitvov is with the School of Physics and Astronomy, Cardiff University, Cardiff, United Kingdom, CF24 3AA.

Y. Xiao is with National Key Laboratory of Science and Technology on Communications, University of Electronic Science and Technology of China, Chengdu, 611731, China.

H. Li is with the Key Laboratory of Radar Imaging and Microwave Photonics, College of Electronic and Information Engineering, Nanjing University of Aeronautics and Astronautics, Nanjing, 210016, China.

wavelength (λ), the resulting arrays are generally large and cannot be readily fitted into small and/or handheld devices; *iii*) since it, like its predecessor LoS-MIMO, relies on LoS links, and nLoS paths are harmful, it can be expected that it could not work properly when LoS paths are blocked and/or when noticeable nLoS paths exist which can be the results of lower operation frequencies, such as X to K frequency bands (8 to 27 GHz), or scattering-rich propagation environments; and *iv*) even if the mmWave frequency is adopted and the LoS links are available and dominant, the high path loss limits the communication range, e.g., the range of only a few meters was considered in [16]–[18].

In order to compensate for these high path losses, and enable systems to operate in nLoS mobile and sparse environment, beamforming gains, ideally at both transmit and receive sides, are required. The required beamforming gains are not possible in standard SM systems since at any time instant only one antenna in an array is activated. This issue can be partly alleviated by using the GSM [7], where a subset of antennas in the array are activated.

We now pose the question '*Is it possible to enable all of the available beamforming gains, i.e., use all the available antennas, instead of a single antenna or a subarray, at any given time, with only one RF chain?*'.

In fact, activating a full array with a single RF feed constitutes the core principle of conventional analog beamforming, whereby the complex weights are generated for each antenna element by a beamforming network inserted between the antenna array and a single RF chain, see Fig. 1. The analog beamforming applied to the conventional SM processing represents the essence of what we term here as *beam index modulation (BIM)*, where the indices of the distinct radiation beams, instead of the indices of the antennas, are used to convey extra information bits. In the most previous hybrid massive MIMO works, an RF analog precoder/beamforming network consisting of an array of variable phase shifters was commonly used [23], [24]. The similar phase shifter-based beamforming network can be adopted for the proposed BIM transmitter, see the bottom-left plot in Fig. 1. However, analog RF phase shifters with fast switching speed and fine resolutions are costly, especially at higher frequencies. This contradicts the main purpose of employing the index modulation schemes. Alternatively, a fixed beamforming network, such as Butler matrix [25] and Fourier Rotman lens [26], together with a switching array, see the bottom-right plot in Fig. 1, can be used to route the single RF chain signal to the entire antenna array, and to project the signal through one of the radiation beams. We could use a single-pole-multi-throw switch to select one of the beam ports, but it, again, is costly for high frequency operations. Thus, the concept proposed in [16] was borrowed. Here an array of single-pole-single-throw switches is used. During any signaling transmission, all switches, but one, stay closed, creating open circuits when seeing from the inputs of the corresponding $\lambda/4$ transmission lines. This architecture is scalable with regard to different numbers of beam ports and has low cost. In addition, with some extra impedance matching, it can be extended for generalized BIM, where more than one radiation beams are activated concurrently for more enhanced spectral efficiency when compared with the single-beam BIM discussed in this paper. This generalized BIM and its potential applications are subject to future studies.

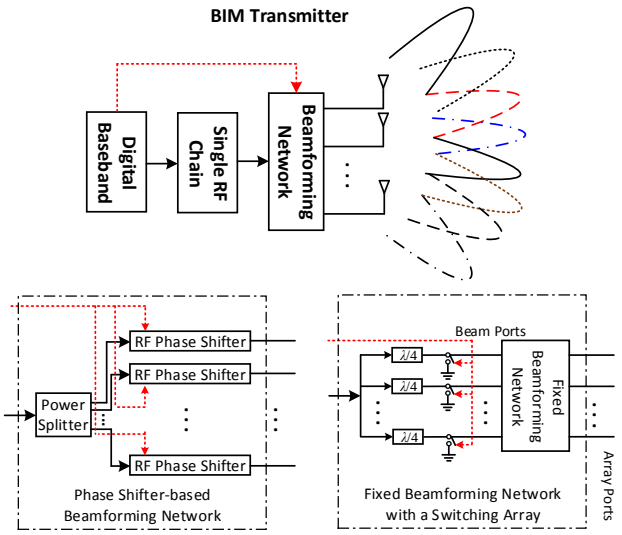

Fig. 1. Architecture of proposed beam index modulation (BIM) transmitter and two optional beamforming networks. The second fixed beamforming network is preferred as it has low cost and design complexity.

In [27] a variant of SM called the spatial scattering modulation (SSM) scheme was proposed. Here the indices of spatial scatterers in nLoS mmWave channels, in fact, correspond to the indices of the generated radiation beams. The investigations of the BIM scheme in this paper, when compared with those for the SSM in [27], provide significantly deeper insight into SSM as well as extending its capabilities, namely;

- The effective operation of the SM requires rich multipath environment, which makes it unsuitable for higher frequency applications where channel matrices can have low ranks and path loss is huge. In order to compensate high path loss and efficiently exploit the sparse nLoS links, analog beamforming networks, which enable all available beamforming gains, are employed at both transmit and receive sides. The indices of the resulting radiation beams, instead of the indices of the transmit antennas in the SM scheme, can, thus, be used to transmit extra information bits, which is the essence of the proposed BIM system;
- The BIM architectures studied in this paper, are applicable to any device-to-device communication systems, whereas the SSM in [27] works only for a single user uplink. This indicates that the proposed BIM here is also applicable to vehicle-to-vehicle communications. The BIM system studied in this paper has a potential to be extended for multi-user applications, which will be investigated in our future works;
  In the proposed BIM architecture, only a single RF chain is required at each communication node, whereas the receive node in the SSM system model requires multiple RF chains [27];
- In addition, more general cases of '*non-orthogonal*' and '*unbalanced beams*', in terms of path loss/gain, are investigated in this paper for the first time;
- Also, the system spectral efficiency is derived and is used here as the metric for quantifying the achievable performance. This performance metric is in contrast to bit error rate (BER), which is modulation dependent, adopted

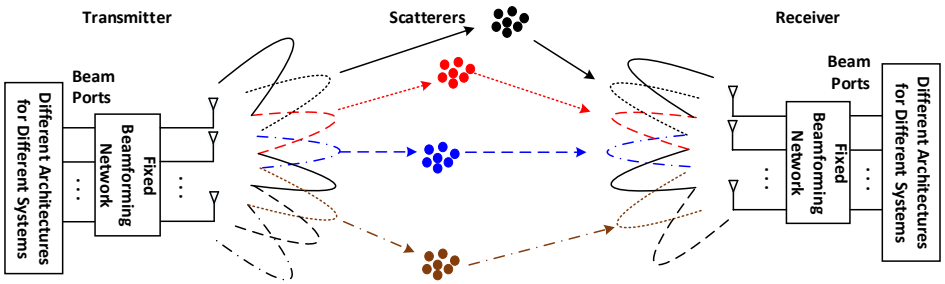

Fig. 2. Illustration of system model, applicable to the proposed BIM, the SSM, and the beam-space (BS) MIMO for the discussions in this paper, operating in nLoS sparse channels in beam domain.

for the SSM performance characterization in [27];

- Some demonstrative calculations based on the measured beam-space channel matrices are provided to substantiate the simulation findings with regard to the applicability of the proposed BIM schemes in various channel conditions.

This paper is organized as follows: in Section II the adopted channel model and underlying system assumptions are introduced. In Section III, the proposed BIM scheme is described, and other various benchmark transmission schemes are also briefly presented. Here the methods of calculating system spectral efficiencies are investigated. Section IV presents extensive simulation results with regard to various channel conditions, leading to conclusions of the general channel condition under which the proposed BIM scheme can be a favorable choice. In Section V, the beam-space channels measured in some indoor environments at 10 GHz are used to validate the findings obtained in the previous section. Finally, conclusions are drawn in Section VI.

II. Channel Model and System Assumptions

It is well known that for a fixed communication distance the wireless propagation path loss in free space is proportional to the square of the operating frequency of the electromagnetic wave. Therefore, for a given noise floor the number of propagation links between single-antenna transmitter and receiver decreases with frequency. For a single antenna operating at a higher frequency, normally only the LoS link is considered because it is much stronger than the other nLoS links that can be close to or even immersed under the system noise floor. In order to combat high path loss, beamforming gain can potentially be enabled by equipping transmitters and receivers with antenna arrays and suitable control electronics as necessary. The availability of beamforming gain can be used to enable the communication system to exploit some of the viable nLoS links. These nLoS links are normally associated with clusters of scatterers that act as relays between the transmit and receive beams, seen in Fig. 2, i.e., thus, resulting in a sparse channel matrix in the beam-space domain.

In this paper, only the case of a flat fading channel is investigated, i.e., the propagation gains of each discernible link between the transmit and receive beams can be represented as a complex number. In addition, the wireless channel is assumed to be quasi-static during the transmission frame, so that the path gains remain constant as well. The above assumption allows direct comparison between the proposed BIM system and the recently reported SSM system [27].

For the SSM work in [27], only the ideal orthogonal beam scenario was investigated and only at the transmit side. Here the term 'orthogonal' means that each of the detectable propagation rays can only be launched by exciting a designated beam port at the input of the beamforming network at the transmit side. In other words, when one propagation link is activated, no signal energy exists in any other propagation links. The beam orthogonality is a special case and is possible only when *a*) through *d*) below occur;

a) the antenna arrays are linear and uniformly half wavelength spaced;

b) the active element patterns of every antenna elements in the array are identical;

c) the beamforming networks function as ideal Fourier transformers between inputs and outputs, e.g., Butler matrix [25] and Fourier Rotman lens [26]; and

d) the clusters of scatterers have small cross-sections and are located along some certain distinct spatial directions, the total number of which is no greater than the number of antenna elements in the array.

Obviously, this set of conditions is very restrictive and unfeasible to attain in practice, so that the systems capable of operating with relaxed requirements for the beam orthogonality become of major interest.

In order to facilitate the discussions in the remaining sections of this paper, the following assumptions or definitions are introduced;

- It is assumed that the knowledge about the propagation links, beam indices at both transmit and receive sides, the propagation path loss (or gain) and phase delay of each link, and the crosstalk (or coupling) between different links (non-orthogonal case), is available and shared at both communication ends. This information can be obtained in the beam training stage, where strategies like exhausted time/beam-sequential training [28], multi-level training [29], and orthogonal codes enabled parallel training [30], can be applied;
- The selected beams at the transmit and receive sides are paired and indexed, and M strongest propagation links are selected. When selecting the strongest links, no beams at either transmit or receive side are re-used in different pairs. Other beam pair selection rules are discussed in Section IV after extensive simulations;
- In order to simplify the BIM receiver architecture and consequent RF hardware requirements, it is assumed that only the power detected at each beam port at the receive side

is used to estimate the indices of the transmit beams. This can be implemented using commonly available power detectors e.g., [31]. This proposed BIM receiver structure is illustrated in Fig. 3, which shares a similar concept as the two-step SM detector described in [32]. This is very different and much simpler to the receivers in the normal SM, where the channel impulse responses associated with each transmit antenna are required by the receivers so that the maximum-likelihood (ML) detection can be performed [33]. The different receive strategies, inevitably, lead to different expressions of the system spectral efficiencies, which will be elaborated in Section III;

- The path loss or path gain of the strongest propagation link enabled by the selected beam pairs is normalized to 0 dB;
- The channel noise associated with each propagation link is assumed to be independent additive white Gaussian noise (AWGN), all following $CN(0, \sigma^2)$;
- The total available transmit power, P_{Tx}, is kept identical when different transmission schemes are considered below, so that fair comparisons can be made and a figure of merit relating the transmit power versus the receive noise power per beam pair, in dB, can be defined as in (1);

$$SNR_{Tx} = 10 \cdot \log_{10}(P_{Tx}/\sigma^2) \tag{1}$$

- In this paper, with regard to the information bits transmitted through modulated RF carriers, it is assumed that the extensively used signaling scheme of zero-mean complex Gaussian (ZMCG) in IQ domain is considered [17], [34]. While for the extra information bits conveyed through beam indices, uniform selections at transmit sides are used.

As discussed above, it is assumed that the channel matrix in the beam domain, denoted as $\boldsymbol{H}^{(b)}$, which has the size of M-by-M, is available at the transmitter and receiver. Its entries are essentially the complex transmission coefficients between the M selected beam ports at the transmit side and the M selected beam ports at the receive side. When appropriately assigning the beam indices, the m^{th} (m = 1, …, M) diagonal entry $h_{mm}^{(b)}$ of $\boldsymbol{H}^{(b)}$ represents the path gain of the m^{th} possible link. Without loss of generality, the beam indices are allocated so that $\left|h_{mm}^{(b)}\right| \geq \left|h_{nn}^{(b)}\right|$ when $m < n$. The operator '$|\cdot|$' takes the modulus of the enclosed complex variable. Since the path gain of the strongest link is normalized to 0 dB, $\left|h_{11}^{(b)}\right| = 1$. The off-diagonal entry $h_{ij}^{(b)}$ ($i \neq j$) of $\boldsymbol{H}^{(b)}$ represents the crosstalk between the i^{th} transmit beam and the j^{th} receive beam.

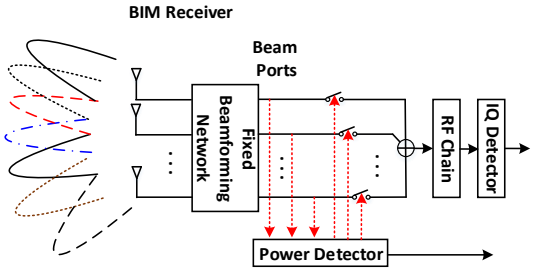

Fig. 3. Illustration of two-step BIM receiver architecture.

III. Beam Index Modulation

In this section, the communication scenario shown in Fig. 2 is investigated. For the BIM scheme, the transmitter and receiver architectures in Fig. 1 and Fig. 3, respectively, exploiting the fixed beamforming networks are considered. The BIM system is also compared with other transmission schemes, some of which employ different structures before/after the fixed beamforming networks at the transmit/receive side. These benchmark systems are elaborated in this and the following sections.

With the availability of the beam-space channel matrix $\boldsymbol{H}^{(b)}$, various transmission strategies associated with different hardware complexity can be used, such as the Beamspace-MIMO (BS-MIMO) [35], [36], conventional beamforming, and the BIM method studied in this paper. In Fig. 4 system architectures before (or after) the fixed beamforming networks at the transmitter (or receiver) for the BS-MIMO and the beamforming transmission schemes are depicted. It is noted that, for the fair comparison, the architecture of fully connected BS-MIMO or beamforming systems using variable phase shifters, seen in [37], is not studied. Instead, the fixed beamforming networks, the same as those adopted in the BIM systems, are employed.

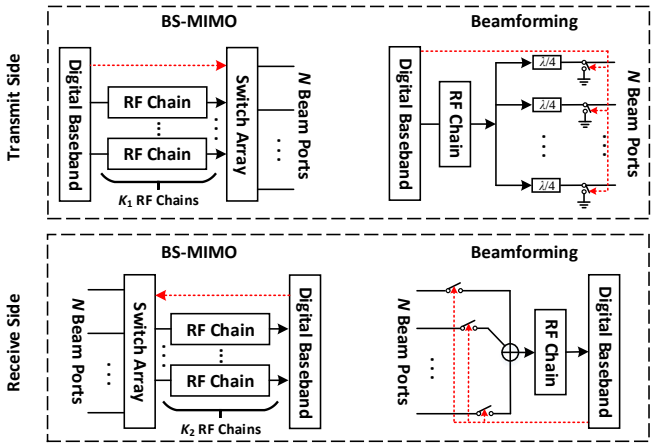

Fig. 4. Transmitter and receiver architectures for BS-MIMO and beamforming used for performance comparison with the proposed BIM communication systems.

In order to implement the BS-MIMO, the number of RF chains are commonly chosen according to the number of dominant propagation paths in the beam domain, which, for the scenario discussed here, equals M. N is the number of the beam ports of the selected beamforming networks, and clearly $M \leq N$. The control signals (dotted arrows in Fig. 4) in the BS-MIMO systems configure the switch arrays so that the M RF chains are connected to the M selected beam ports that correspond to the selected M strongest beam pairs. In Fig. 4, it can be seen that the architecture of the beamforming system is nearly identical to that of the BIM system shown in Fig. 1 and Fig. 3, because both schemes require only one RF chain at transmit and receive sides. However, it has to be pointed out that the switch controlling signals, namely the dotted arrows, in the beamforming systems are updated at the channel fading rates, instead of at the symbol rates in the BIM systems. Thus, no information bits can be transferred through the switch

configurations in the beamforming systems. In the beamforming system, the strongest beam pair is always selected for transmission.

In contrast to the BS-MIMO and the beamforming systems, in the proposed BIM system, at the transmit side the control signal dynamically, at the transmitted symbol rate, routes the single RF signal to one of the pre-selected M beam ports. The changing patterns of the transmit beam indices are determined by the baseband data, $\log_2(M)$ bits, which are additional control information transmitted alongside the information data applied upon the RF carriers in IQ domain. At the receive side, a simple power detector array of size M-by-1 is used to identify, based on the strongest receive power, the receive beam index that is paired with the transmit beam index in the beam training stage. Thus, the single RF chain is connected to the receive beam of the recovered beam index. In the meantime, the receive beam indices are processed in the digital baseband in order to extract the transmitted $\log_2(M)$ control information bits. From a practical point of view, RF switches capable of operating at nanosecond or even sub-nanosecond speeds are commercially feasible, [38] and [39], and can be used directly in the BIM systems.

In the SSM system proposed in [27], the receiver equips multiple RF chains to perform joint ML detection. In order to facilitate comparison with the BIM system, we assume that the SSM receiver employs M RF chains, which are connected to the M beam ports of the fixed beamforming networks the same as those used in the BIM receiver.

Given all four transmission schemes, namely the BS-MIMO, the beamforming, the SSM, and the BIM, use the same fixed beamforming networks at both transmit and receive sides, the beam-space channel matrix $\boldsymbol{H}^{(b)}$ is directly applicable. Thus, in the following, we first present or derive the spectral efficiencies of these four schemes, in bits per channel use (*bpcu*), leaving the comparison studies to the SMX-MIMO and the SM systems that rely on the channel matrices in antenna domain later in this section.

- *BS-MIMO*

When M RF chains are connected to the M beam ports associated with the M selected strongest beam pairs, the conventional MIMO processing, based upon the M-by-M channel matrix $\boldsymbol{H}^{(b)}$ in the beam domain, can be used. The spectral efficiency of the BS-MIMO system can, thus, be expressed as, [40],

$$SE_{BS} = \sum_{m=1}^{M} \log_2\left(1+\mu_m \frac{\lambda_m^2}{\sigma^2}\right), \tag{2}$$

where λ_m is the m^{th} singular value of the matrix $\boldsymbol{H}^{(b)}$, and μ_m is its associated water-filling power allocation coefficient.

- *Beamforming*

When only one RF chain is available at both transmit and receive sides, the best strategy for beamforming is to select the beam pair of the highest path gain for transmission, which in the channel model with normalized path gains considered in this paper is 0 dB. In this case, the spectral efficiency for the beamforming system is

$$SE_{BF} = \log_2\left(1+\frac{P_{Tx}\cdot 1}{\sigma^2}\right) = \log_2\left(1+SNR_{Tx}\right). \tag{3}$$

- *SSM*

In order to facilitate fair comparison with the proposed BIM scheme, it is assumed that the both transmit and receive sides are equipped with the fixed beamforming networks the same as those used in the BIM systems. Since joint ML detection is adopted, the capacity calculation methods developed for ML SM can be directly used for the SSM, by simply replacing the antenna domain channel matrices with the beam domain channel matrices. In [41], [42], the integral-based expressions of the instantaneous SM capacity, for ZMCG signaling in IQ domain and uniform selection in index domain, were presented. Later, its closed-form approximation was derived in [43]. In this paper, we adopt the 4^{th} order approximation, i.e., (29) in [43]. To keep a cohensive presentation in this paper, we re-write it in (4),

$$SE_{SSM} \;;\; \log_2\left(B\left(\boldsymbol{\eta}^2\right)\right) - \frac{1}{\ln(2)}\left[1-A\left(\boldsymbol{\eta}^2\right)\frac{B\left(\boldsymbol{\eta}^2\right)}{B\left(\boldsymbol{\eta}^4\right)} + \frac{3}{4}A\left(\boldsymbol{\eta}^4\right)\left(\frac{B\left(\boldsymbol{\eta}^2\right)}{B\left(\boldsymbol{\eta}^6\right)}-\frac{B^2\left(\boldsymbol{\eta}^2\right)}{B^2\left(\boldsymbol{\eta}^4\right)}\right)\right]. \tag{4}$$

$\boldsymbol{\eta}^k$ in (4) denotes a vector $\left[\eta_1^k \quad \eta_2^k \quad \mathrm{L} \quad \eta_M^k\right]^T$, where $\eta_m = \sqrt{1+\gamma_m\left\|\boldsymbol{h}_m^{(b)}\right\|^2}$. $\boldsymbol{h}_m^{(b)}$ refers to the m^{th} column of the beam-space channel matrix $\boldsymbol{H}^{(b)}$, and γ_m is the receive SNR when the m^{th} beam pair is selected for transmission. Operators '$[\cdot]^T$' and '$\|\cdot\|$' perform vector transpose and 2-dimensional Euclidean norm. $A(\cdot)$ and $B(\cdot)$ are the arithmetic and harmonic mean operators, respectively.

- *BIM*

In the BIM communication scheme, in addition to the information transmitted through the RF carriers propagated along the selected beam pairs, the activated transmit beam indices, when correctly identified at the receive side, can be used to convey additional information. One propagation path is utilized per channel use. Different to the SSM scheme where the joint ML detection is adopted, the proposed BIM receiver performs the two-step detection, see the architecture in Fig. 3, i.e., identifying the beam indices first according to the received signal power at each beam port, and then recovering the information conveyed by the signal in IQ domain received at the identified beam port. Different detection schemes inevitably result in different system spectral efficiencies.

We first investigate the information transferred through the beam indices, which is the first step that a proposed BIM receiver performs. At the transmit side, each transmit beam is equally selected. And the receiver identifies the beam indices solely based on the strongest instantaneous power. This process can be modeled as a transmission through a discrete input (transmit beam indices) discrete output (receive beam indices)

channel. Thus, the associated spectral efficiency can be calculated as in [44], [45]

$$SE_{BIM1} = \frac{1}{M}\sum_{i=1}^{M}\sum_{j=1}^{M} p_{ij}\log_2\left[p_{ij}\Big/\left(\frac{1}{M}\sum_{s=1}^{M} p_{sj}\right)\right], \quad (5)$$

where p_{xy}, forming a probability matrix $\boldsymbol{P}$, represents the probability of the receiver selecting the y^{th} receive beam when the x^{th} transmit beam is used for transmission.

In the second step, the only receive RF chain is connected to the receive beam port identified in the first step and recovers the information applied in IQ domain. This associated spectral efficiency is generally lower than that in beamforming systems, because *i*) beam pairs with lower path gains are equally used for transmissions in the BIM, in contrast to the conventional beamforming using the strongest link all the time, and *ii*) in the BIM architecture there is a chance that the receiver cannot identify the correct transmit beam indices due to the channel noise presented in the systems. This partial BIM spectral efficiency can be expressed as

$$\begin{aligned} SE_{BIM2} &= \frac{1}{M}\sum_{i=1}^{M}\left[p_{ii}\log_2\left(1+\frac{\left|h_{ii}^{(b)}\right|^2 P_{Tx}}{\sigma^2}\right)\right] \\ &\quad + \frac{1}{M}\sum_{i=1}^{M}\sum_{j=1,j\neq i}^{M}\left[p_{ij}\log_2\left(1+\frac{\left|h_{ij}^{(b)}\right|^2 P_{Tx}}{\sigma^2}\right)\right] \\ &= \frac{1}{M}\sum_{i=1}^{M}\left[p_{ii}\log_2\left(1+\left|h_{ii}^{(b)}\right|^2 SNR_{Tx}\right)\right] \\ &\quad + \frac{1}{M}\sum_{i=1}^{M}\sum_{j=1,j\neq i}^{M}\left[p_{ij}\log_2\left(1+\left|h_{ij}^{(b)}\right|^2 SNR_{Tx}\right)\right]. \end{aligned} \quad (6)$$

The first term on the right-hand side of (6) corresponds to the information transmitted through the correct beam pairs, while the second term reveals that even when the receiver selects a wrong beam, i.e., $j \neq i$, a certain amount of transmitted information can still be recovered if crosstalk among beam pairs exists, i.e., $\left|h_{ij}^{(b)}\right| \neq 0$.

Now we elaborate how the probability matrix $\boldsymbol{P}$ can be calculated. It needs to be pointed out that SE_{BIM2} in (6) can be achieved only when the input signal of power P_{Tx} is ZMCG distributed, as it is assumed in this paper. As a consequence, when the signal is projected through the i^{th} transmit beam, the received signal through the j^{th} receive beam v_{ij} follows $CN\left(0,\left|h_{ij}^{(b)}\right|^2 P_{Tx}+\sigma^2\right)$. In our proposed two-step BIM receiver architecture in Fig. 3, in order to maintain low hardware complexity, as we discussed in Section II, only the power of the detected signals at the beam ports at the receive side is used for beam selection. Thus, only $|v_{ij}|^2$ are available. Following the definition,

$$p_{ij} = p\left[\mathop{\mathrm{I}}_{s\in[1,\mathrm{K},M]}^{s\neq j}\left(\left|v_{ij}\right|^2 > \left|v_{is}\right|^2\right)\right]. \quad (7)$$

Here '$p[\cdot]$' stands for the probability of the enclosed event, and '$\cap$' denotes the joint of the events. When M is greater than 2, events for different s are statistically dependent, and there is no closed-form expression for the p_{ij} calculation. Only when $M = 2$ and $h_{12}^{(b)} = h_{21}^{(b)} = 0$, closed-form expression for (7) exists, see Appendix for further details. In general, p_{ij} can be obtained through Monte Carlo simulations. It is also noted that $\sum_{j=1}^{M} p_{ij} = 1$.

After the probability matrix $\boldsymbol{P}$ has been calculated, the overall spectral efficiency of the BIM system can be obtained by adding up the information transmitted through the selected beam pairs and their indices, namely,

$$SE_{BIM} = SE_{BIM1} + SE_{BIM2}. \quad (8)$$

In order to provide readers a bigger picture of how the BIM performs, we also construct the SMX-MIMO and the SM systems, which rely on the channel matrix $\boldsymbol{H}^{(a)}$ in the antenna domain. To facilitate discussion, it is assumed that both transmitter and receiver equip the same fixed beamforming networks with the transfer matrix $\boldsymbol{T}$ of size N-by-N. N is also the number of antennas, and clearly, $N \geq M$. The $\boldsymbol{H}^{(a)}$ can be computed via

$$\boldsymbol{H}^{(a)} = \boldsymbol{T}^{-1}\bar{\boldsymbol{H}}^{(b)}\left(\boldsymbol{T}^{T}\right)^{-1}, \quad (9)$$

where $\bar{\boldsymbol{H}}^{(b)}$ is the extended beam-space channel matrix of the size N-by-N, i.e., $\boldsymbol{H}^{(b)}$ is the sub-matrix of $\bar{\boldsymbol{H}}^{(b)}$. '$(\cdot)^{-1}$' refers to the inverse of the enclosed matrix.

With the availability of the $\boldsymbol{H}^{(a)}$, the spectral efficiencies of the SMX-MIMO, SE_{MIMO}, and the SM, SE_{SM}, can, thus, be calculated by replacing the relevant parameters, i.e., μ_m, λ_m, and $\boldsymbol{\eta}$, in (2) and (4) with the corresponding ones that are derived from the $\boldsymbol{H}^{(a)}$.

It is noted that all the analyses in this section are based on the assumption of flat fading channels, which was stated in Section II. In the case of frequency selective wireless channels, inter-symbol interference (ISI) occurs. Thus, when replacing σ^2 with $(\sigma^2 + \rho^2)$, where ρ^2 denotes the power of ISI, equations (2) to (8) are also applicable to the corresponding schemes in frequency selective channels. The value of ρ^2 is determined by the relationship between the signal bandwidth and the channel's coherence bandwidth. The study of the performance of the proposed BIM system in frequency selective channels will be presented separately in our future work.

IV. Simulation Results

Using (2), (3), (4), and (8), the spectral efficiencies for the BS-MIMO, the beamforming, the SSM, and the proposed BIM transmission schemes, all of which exploit beam-space channel matrix $\boldsymbol{H}^{(b)}$, are simulated and plotted in Fig. 5 (a) to (d). Here only two orthogonal beam pairs, i.e., $M = 2$ and $h_{12}^{(b)} = h_{21}^{(b)} = 0$, are considered. The path gain difference Δg, in dB, in Fig. 5 is defined as

$$\Delta g = 20\cdot\log_{10}\left(\left|h_{11}^{(b)}\right|\Big/\left|h_{22}^{(b)}\right|\right). \quad (10)$$

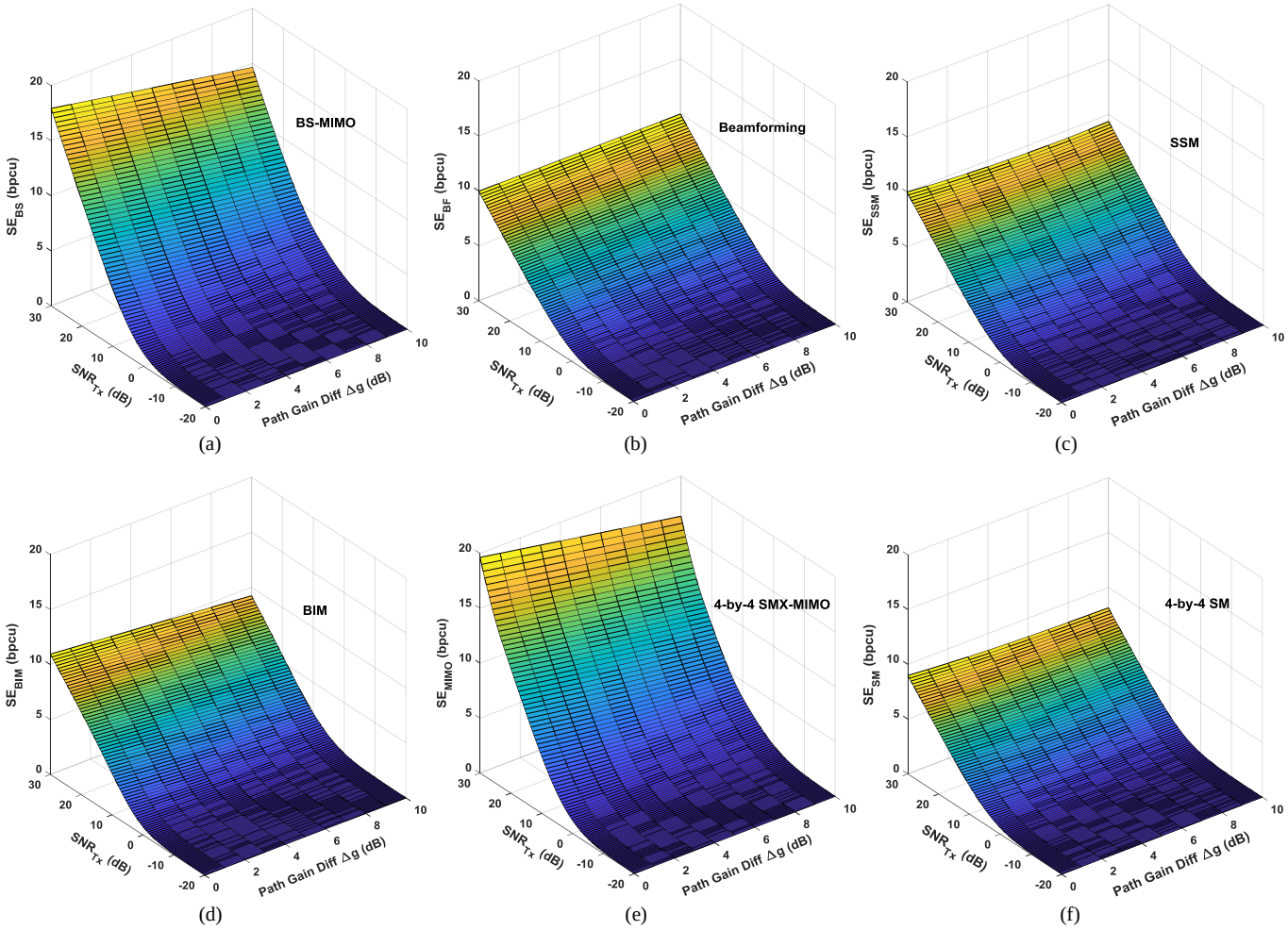

Fig. 5. Calculated spectral efficiencies for (a) BS-MIMO, (b) beamforming, (c) SSM, (d) BIM, (e) 4-by-4 SMX-MIMO, and (f) 4-by-4 SM systems as functions of SNR_{Tx} and path gain differences Δg, when two orthogonal beam pairs are available. It is assumed that in the BIM systems the 4-by-4 Fourier beamforming networks ($N = 4$) are used at both transmit and receive sides, and the remaining $N - M = 2$ orthogonal beam pairs have identical normalized path gains of –20 dB. Thus, this extended channel matrix in beam domain $\bar{\boldsymbol{H}}^{(b)}$ can be used to calculate channel matrix in antenna domain $\boldsymbol{H}^{(a)}$ via (9), which is then exploited to construct the 4-by-4 SMX-MIMO and the 4-by-4 SM systems for comparison.

In order to evaluate the performance of the SMX-MIMO and the SM systems for comparison, which rely on the channel matrix $\boldsymbol{H}^{(a)}$ in antenna domain, some assumptions have to be made to construct the extended beam-space channel matrix $\bar{\boldsymbol{H}}^{(b)}$, which, in turn, is used to calculated $\boldsymbol{H}^{(a)}$ via (9). Here, we assume that 4-by-4 Fourier beamforming networks are used at both transmit and receive sides in the discussed BIM systems, i.e., $N = 4$ and the $(u, v)^{th}$ entry in the matrix $\boldsymbol{T}$ is expressed as $\left(1/\sqrt{N}\right)\cdot\exp\left\{-j\,2\pi\left[u-\left(N+1\right)/2\right]\left[v-\left(N+1\right)/2\right]/N\right\}$, and the remaining $N - M = 2$ orthogonal beam pairs have identical normalized path gains of –20 dB, i.e., $20\cdot\log_{10}\left(\left|h_{33}^{(b)}\right|\right) = 20\cdot\log_{10}\left(\left|h_{44}^{(b)}\right|\right) = -20$. With the availability of the $\boldsymbol{H}^{(a)}$, the calculated spectral efficiencies of the 4-by-4 SMX-MIMO and the 4-by-4 SM systems are also plotted in Fig. 5.

The observations from the Fig. 5 are summarized as below;

- The 4-by-4 SMX-MIMO system has the optimal performance at the cost of 4 RF chains at both transmit and receive sides;
- The BS-MIMO scheme, exploiting the Fourier beamforming networks to transform the propagation channel from the antenna domain into the beam domain, has the sub-optimal performance in the considered sparse channel scenario. By neglecting the two path links of –20 dB gain only two RF chains are required, instead of 4 used in the SMX-MIMO system, at the cost of around 2 *bpcu* spectral efficiency loss at 30 dB SNR_{Tx};
- The single-beam beamforming system always projects signals along the strongest beam pair, in this example, of 0 dB normalized gain. Thus, it is independent to Δg;
- The 4-by-4 SM system, as expected, performs the worst in the considered sparse channel as no beamforming gains are available. In particular, the superior of the proposed BIM over the 4-by-4 SM is graphed in Fig. 6 (a);
- Under this ideal orthogonal beam-space channel condition, the joint ML detection used in the SSM scheme does not help increase the spectral efficiency compared with the beamforming scheme when the transmitted signals in IQ domain are ZMCG distributed and the different beam pairs are uniformly selected. This is consistent to the findings obtained in [41], i.e., the first term on the right-hand side in (4), equivalent to (6) in [41],

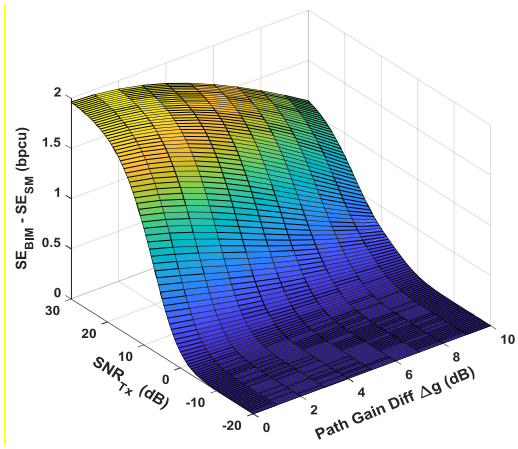

(a)

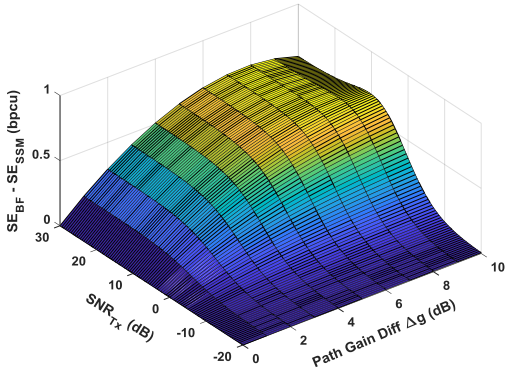

(b)

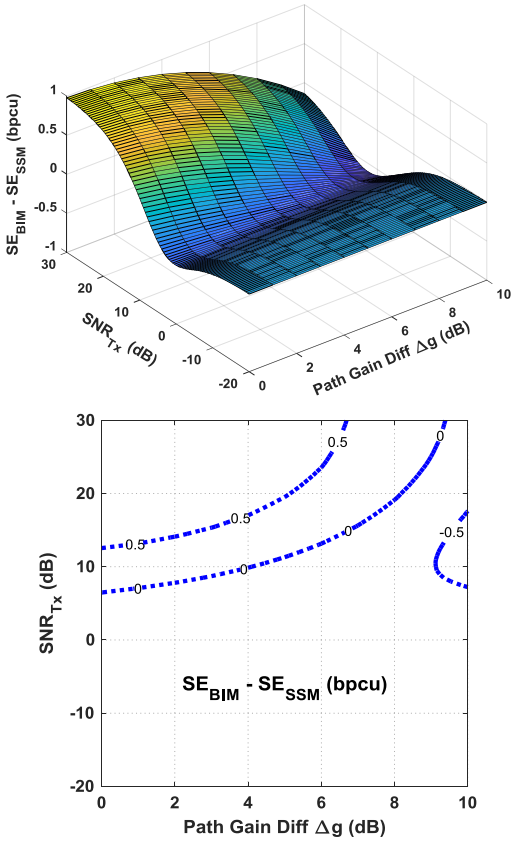

(c)

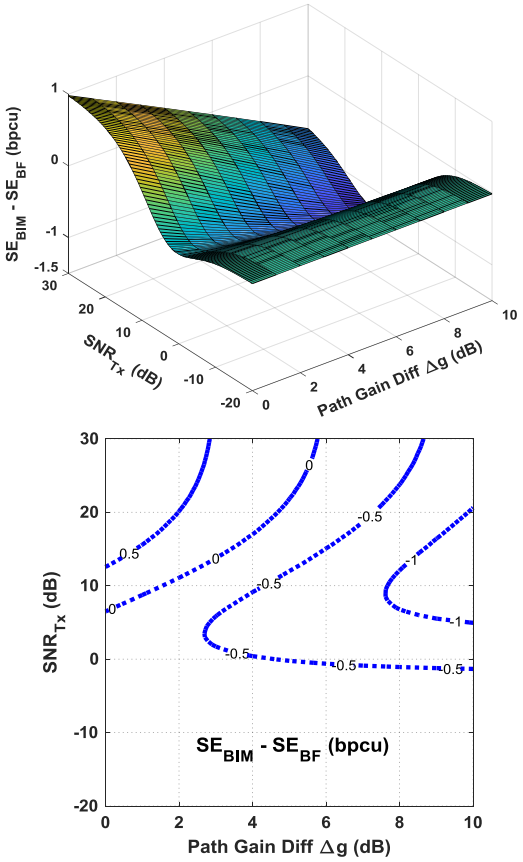

(d)

Fig. 6. Differences in spectral efficiencies, calculated and shown in Fig. 5, (a) between the BIM and the 4-by-4 SM systems, (b) between the beamforming and the SSM systems, (c) between the BIM and the SSM systems, and (d) between the BIM and the beamforming systems.

is smaller than the SE_{BF} in (3), equivalent to (12) in [41], and the second term on the right-hand side in (4), equivalent to (10) in [41], is extremely small in ideal orthogonal channel scenarios, which is evidenced in Fig. 3 in [41] where the overall spectral efficiency barely increases with the increase of the dimension in index domain. As a consequence, the beamforming scheme outperforms the SSM scheme, see Fig. 6 (b). It is noted here that when the channels are not orthogonal, the second term on the right-hand side in (4) becomes much larger, making SE_{SSM} greater than SE_{BF} under some channel conditions. This aspect will be discussed later in this section. It also needs to point out that the scenario discussed here is different to the case when the IQ domain signals are PSK or QAM modulated, where an additional $\log_2(M)$ *bpcu* spectral efficiency can be obtained in high SNR region by the index modulation system compared with that in the single-beam beamforming system [42];

- The proposed two-step detection BIM system with only one RF chain can achieve better spectral efficiency compared with the ML SSM system in high SNR_{Tx} and low Δg regions, see Fig. 6 (c). When comparing the BIM with the beamforming scheme, which has similar hardware complexity, the BIM system, again, exhibits higher spectral efficiency in high SNR_{Tx} and low Δg regions, see

Fig. 6 (d). In the extreme condition of SNR_{Tx} = 30 dB and Δg = 0, an extra 1 *bpcu* is achieved via the information conveyed through the two beam pair indices, i.e., $\log_2(M)$ = 1. Intuitively, when more beam pairs are available, even higher spectral efficiency gains, (SE_{BIM} – SE_{SSM}), and (SE_{BIM} – SE_{BF}), can be obtained in the same high SNR_{Tx} and low Δg region, see the example for four orthogonal beam pairs in Fig. 7.

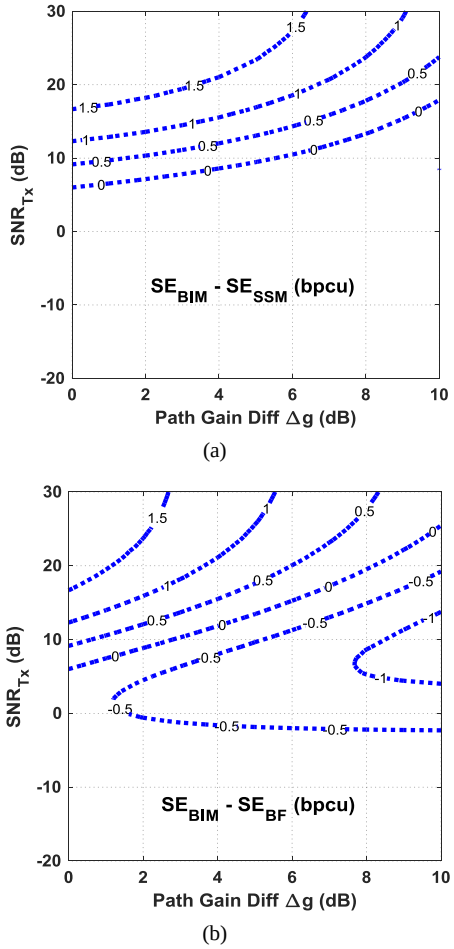

Fig. 7. Contour plots of the differences in the calculated spectral efficiencies, (a) between the BIM and the SSM systems, and (b) between the BIM and the beamforming systems when four orthogonal beam pairs are available. It is assumed that $\left|h_{11}^{(b)}\right|^2 = \left|h_{22}^{(b)}\right|^2 = 1$, and $\left|h_{33}^{(b)}\right|^2 = \left|h_{44}^{(b)}\right|^2 = 10^{-\Delta g/10}$.

As we discussed in Section II, in general, the available beam pairs are not necessarily orthogonal, so that we expect the beam crosstalk to reduce the probability p_{ii} of correctly identifying the beam indices at receive side. This should, in turn, decrease the achievable spectral efficiency in the BIM system. Fortunately, from the simulated (SE_{BIM} – SE_{BF}) in the two-beam scenario shown in Fig. 8, we can conclude that in the high SNR_{Tx} region, the SE_{BIM} is not sensitive to the beam pair crosstalk $\Delta\beta$, when $\Delta\beta$ is lower than –3 dB. The same conclusions can be drawn for more available beam pairs, of which the results are, thus, omitted here. For the examples in Fig. 8, we assume that the beam crosstalk $\Delta\beta_{ij}$, defined in (11), for all i and j combinations are identical and are termed as $\Delta\beta$.

$$\Delta\beta_{ij} = 20 \cdot \log_{10}\left(\left|h_{ij}^{(b)}\right| \Big/ \left|h_{ii}^{(b)}\right|\right). \qquad (i \neq j) \qquad (11)$$

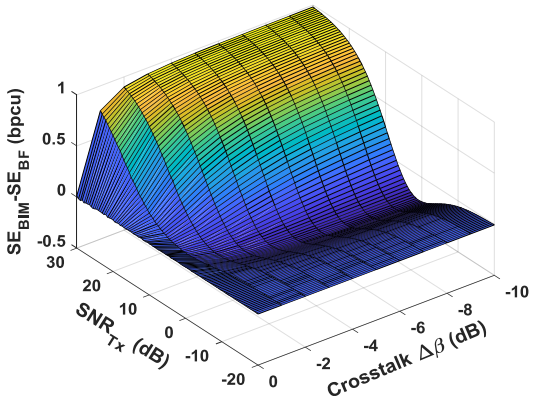

Fig. 8. The differences between the calculated spectral efficiencies of the BIM and the beamforming systems as functions of SNR_{Tx} and crosstalk $\Delta\beta$ when two non-orthogonal beam pairs are available. It is assumed that $\left|h_{11}^{(b)}\right|^2 = \left|h_{22}^{(b)}\right|^2 = 1$.

The existence of the beam crosstalk in the propagation channels can favor both the SSM and the SM schemes, though through different physical mechanisms. For the SSM, the multiple RF chains in the ML receiver are able to harvest a greater amount of signal energy when the beam crosstalk, namely, energy coupling, occurs in the channel, see an example in Fig. 9, where $\Delta\beta$ of 0 dB in two-beam scenario results in 3 dB SNR improvement. While for the SM, the higher crosstalk among the beam pairs indicates that there are more scatterers in the propagation environment, namely, the channel matrix is less sparse. As a consequence, the multipath components could assist the SM scheme to achieve higher spectral efficiency [6]. In the SM example shown in Fig. 10, the same assumptions are used as those associated with Fig. 5 (f) except for Δg = 0 and $\Delta\beta \neq 0$. It can be seen that, as expected, the SE_{SM} increases as the beam crosstalk $\Delta\beta$ gets larger.

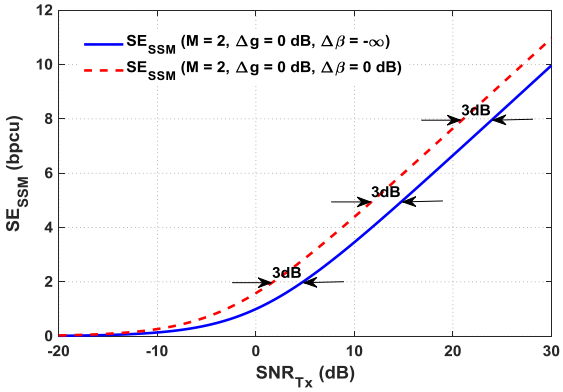

Fig. 9. Examples of calculated SE_{SSM} when the beam crosstalk $\Delta\beta$ are set to be $-\infty$ and 0 dB, respectively. It is assumed that M = 2 and Δg = 0 dB.

In order to illustrate how the proposed BIM performs compared with the SSM and the SM systems when beam pairs are not orthogonal, the (SE_{BIM} – SE_{SSM}) and (SE_{BIM} – SE_{SM}) are, respectively, plotted in Fig. 11 (a) and (b). The same conclusions can be obtained, which are *i*) the BIM performs better in high SNR and low beam crosstalk channels; *ii*) the

SSM, at the cost of multiple receive RF chains, and the SM perform better in high (or medium) SNR and high (or medium) beam crosstalk channel conditions; and *iii*) in low SNR channel environment, there are no noticeable performance differences among these three different transmission schemes.

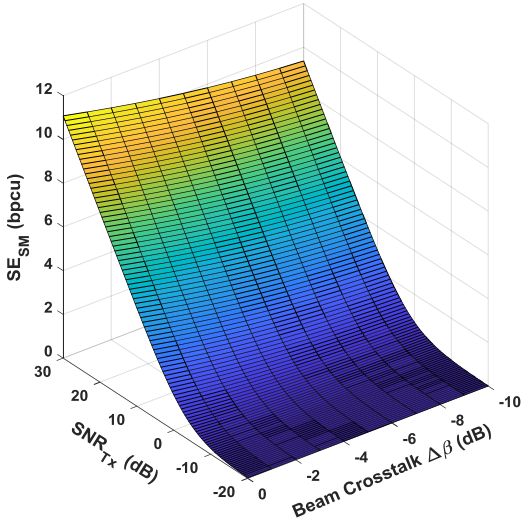

Fig. 10. Example of calculated spectral efficiency of the 4-by-4 SM system as a function of SNR_{Tx} and beam crosstalk $\Delta\beta$. It is assumed that $N = 4$, $M = 2$, $\Delta g = 0$ dB, and the remaining $N - M = 2$ beam pairs have identical normalized path gains of –20 dB.

From the studies in this section we may conclude that in order to achieve better performance against the beamforming, the SSM, and the SM systems, the BIM scheme should follow some basic rules below for selecting the feasible beam pairs. These rules, in other words, provide guidelines for system designers to choose different transmission schemes according to various channel conditions.

- The path gains of the selected beam pairs need to be high, which leads to high SNR, see Fig. 6 (a) (c) (d), Fig. 7, and Fig. 11;
- The path gain differences among the selected beam pairs need to be small, see Fig. 6 (a) (c) (d) and Fig. 7. This requirement violates the LoS channel condition, indicating the BIM scheme should only be selected for some nLoS transmissions;

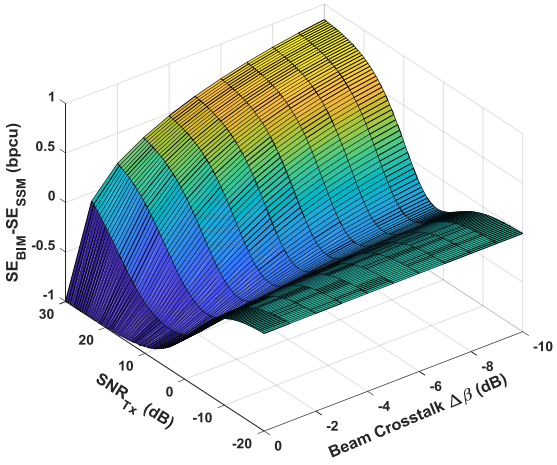

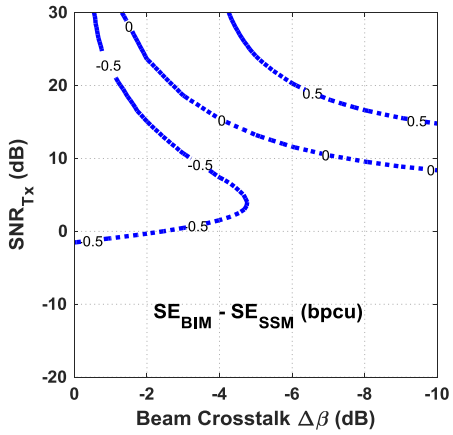

(a)

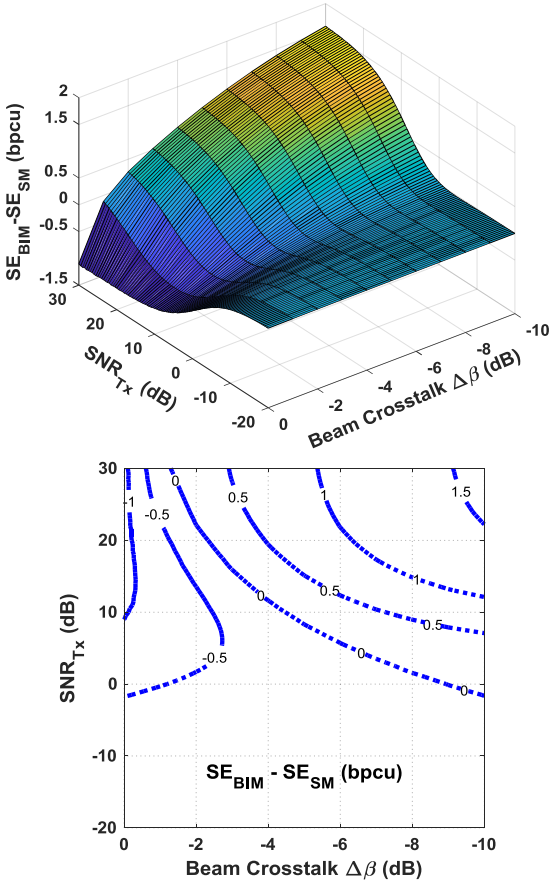

(b)

Fig. 11. The differences between the calculated spectral efficiencies of the BIM system and (a) the SSM system, (b) the 4-by-4 SM system shown in Fig. 10 as functions of SNR_{Tx} and crosstalk $\Delta\beta$ when two non-orthogonal beam pairs are available. It is assumed that $\left|h_{11}^{(b)}\right|^2 = \left|h_{22}^{(b)}\right|^2 = 1$.

- When the above two conditions are met, greater number of available beam pairs results in more enhanced BIM performance, see Fig. 6 (c) (d) and Fig. 7;
- In general, the BIM system performance is not severely degraded when the crosstalk among different beam pairs is lower than –3 dB, see Fig. 8;
- Under high SNR and low beam crosstalk channel conditions,

the BIM outperforms the corresponding SSM and SM systems, see Fig. 11.

V. Experimental Results

In this section, by using a 13-by-13 Fourier Rotman lens and a 13-element linear microstrip patch antenna array designed for 10 GHz operation, [46], the beam-space channel matrices have been measured in some indoor lab environments. From these channel matrices, the achievable spectral efficiencies for the various systems, including the proposed BIM scheme, are calculated using the equations presented in Sections III.

The choice of the 10 GHz measurement is partly because of the availability of the analog beamforming networks and the associated antenna arrays. More importantly, for this 'middle-range' operation frequency, both multipath-poor (sparse) and multipath-rich propagation channels can be created by carefully setting the indoor scattering environment, facilitating the validation of the conclusions summarized in the end of Section IV.

The photograph of the fabricated antenna front-end, comprising a Fourier Rotman lens beamforming network and a linear patch antenna array is shown in Fig. 12. The details of their measured performance, such as S-parameters, antenna active element patterns, and radiation beam patterns generated by exciting each beam port of the Fourier Rotman lens, can be found in [46]. When positioning two communication nodes, equipped with the same antenna front-ends, in the first test indoor environment, also shown in Fig. 12, the 13-by-13 beam-space channel matrix at 10 GHz was measured, and the power of each entry is plotted in Fig. 13. There are few scatterers in the propagation environment, resulting in a sparse beam-space channel matrix evidenced in Fig. 13. The boresight of the two arrays was deliberately aligned and unblocked, so that $h_{77}^{(b)}$ corresponds to the LoS link, of which the path gain is

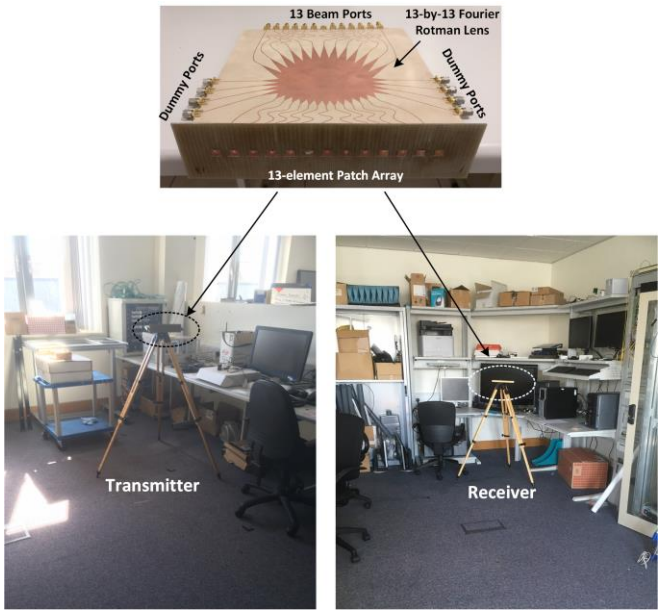

Fig. 12. Photograph of the fabricated 13-by-13 Fourier Rotman lens and the attached 13-element linear microstrip patch antenna array for 10 GHz operation, and a photograph of an indoor multipath-poor lab environment where the channel measurement was conducted.

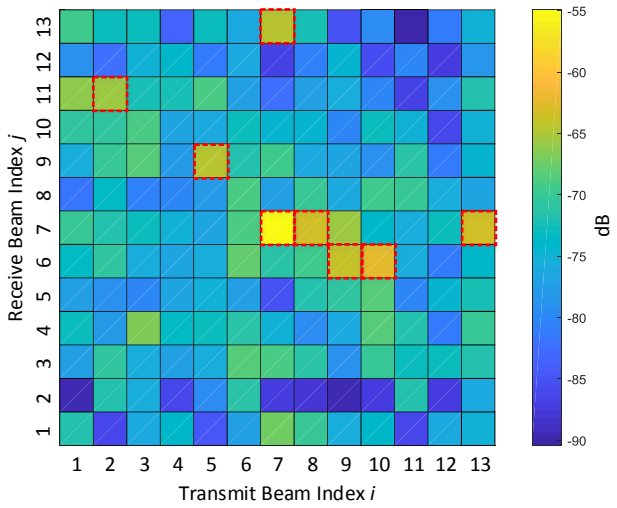

Fig. 13. Measured beam-space $\left|h_{ij}^{(b)}\right|$ in dB, at 10 GHz, when two identical communication nodes, each equipped with a 13-by-13 Fourier Rotman lens and a linear 13-element patch array, were placed in the indoor lab environment shown in Fig. 12.

at least 7.3 dB higher than those of other beam pairs, see Table I. For readability, in this section we do not re-assign the beam indices to construct the channel matrix $\boldsymbol{H}^{(b)}$, but to use those in Fig. 13.

Under the channel state shown in Fig. 13, when the beamforming strategy is selected, the strongest LoS link $h_{77}^{(b)}$ should always be used. Conversely, when the proposed BIM scheme is implemented, the achievable spectral efficiency is determined by the number of available beam pairs and how they are selected. Following the general rules of the beam-pair selection, investigated in the last section, we choose the beam pairs (i, j) of $\{(7, 7); (10, 6)\}$ and $\{(7, 7); (10, 6); (5, 9); (2, 11)\}$, respectively, to construct two-beam and four-beam BIM systems. With the measured $\boldsymbol{H}^{(b)}$ and the measured transfer function of the 13-by-13 Fourier Rotman lens, the antenna domain 13-by-13 channel matrix $\boldsymbol{H}^{(a)}$ can be obtained using (9). Thus, if a 13-by-13 SM system is constructed, its spectral efficiency can be calculated using (4) by replacing the relevant parameters with their counterparts derived from $\boldsymbol{H}^{(a)}$.

TABLE I
First Eight Greatest $\left|h_{ij}^{(b)}\right|$ (in dB) in the Measured Beam-space Channel Matrix Shown in Fig. 13. These Eight Beam Pairs are Enclosed in Fig. 13.

i	j	$20\log_{10}\left\|h_{ij}^{(b)}\right\|$	$20\log_{10}\left\|\hat{h}_{ij}^{(b)}\right\|$ (Normalized)
7	7	–54.9 dB	0 dB
10	6	–62.2 dB	–7.3 dB
8	7	–63.3 dB	–8.4 dB
13	7	–63.5 dB	–8.6 dB
9	6	–64.2 dB	–9.3 dB
5	9	–64.4 dB	–9.5 dB
7	13	–64.8 dB	–9.9 dB
2	11	–65.5 dB	–10.6 dB

The spectral efficiencies of the beamforming, the 13-by-13

SM, and the BIM systems with the selected beam pairs, always including the LoS link, have been calculated and are shown in Fig. 14. Here normalized channel coefficients, referenced to the $h_{77}^{(b)}$, were used, and the highest beam crosstalk level is around –4 dB. We fist compare these three transmission schemes because all of them require only one RF chain. It can be seen that when the LoS link is available, the beamforming system performs best in the whole SNR region among these single RF chain schemes. Though with 13 antenna indices available, the SM system, in general, performs the worst, because the propagation channel is multipath-poor, seen in Fig. 13, and no beamforming gain is available. Also, it can be concluded that in the LoS environment increasing the number of selected beam pairs reduces the BIM spectral efficiency. This is because the increase of the spectral efficiency associated with the beam indices, e.g., SE_{BIM1} term in (5) increases from 0.96 to 1.81 *bpcu* at SNR_{Tx} of 30 dB when four beam pairs are used, instead of two, is insufficient to compensate the spectral efficiency loss of SE_{BIM2} in (6) due to the lower percentage, from 50% to 25%, of transmitting signal energy through the strongest LoS link, e.g., SE_{BIM2} reduces from 8.75 to 7.65 *bpcu* under the same condition. In Fig. 15 the two-beam BIM system is also compared with the corresponding BS-MIMO and SSM systems. It is noted that the BS-MIMO requires two RF chains at both transmit and receive sides, and the SSM system needs one transmit RF chain but two receive RF chains. As expected, the BS-MIMO exhibits superior performance. However, the SSM system, though performing joint ML detection with two receive RF chains, has a similar spectral efficiency with that of the BIM system. The comparisons among the four-beam BIM, the four-beam SSM, and the 4-by-4 BS-MIMO are omitted as the same conclusion can be drawn.

In the case when the LoS link is not available, e.g., being blocked, it is expected that, as illustrated in Fig. 16, the BIM systems exhibit some performance advantage over the beamforming and the SM systems in the high SNR region. This is consistent with the observations made in Section IV. In

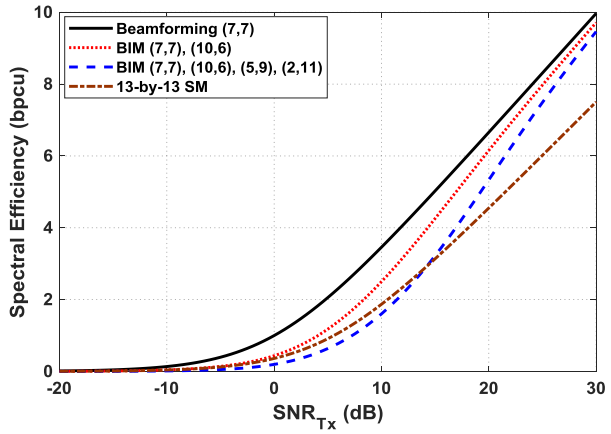

Fig. 14. Calculated spectral efficiencies of the beamforming, the 13-by-13 SM, and the BIM systems, based on the measured channel matrix shown in Fig. 13, when the LoS link $h_{77}^{(b)}$ is available. Two or four beam pairs, respectively, are selected for the BIM system with transmit and receive beam index pairs (*i*, *j*) labelled in the legends.

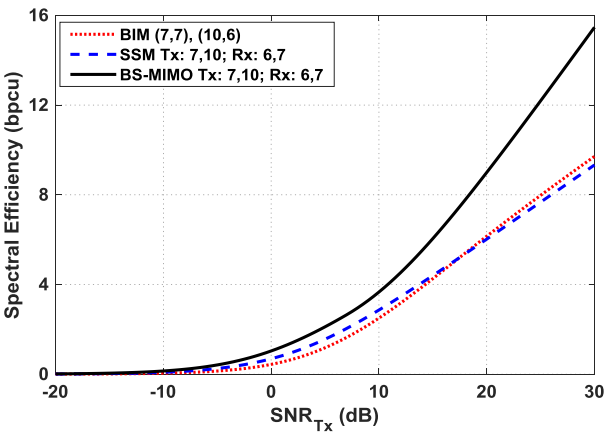

Fig. 15. Calculated spectral efficiencies of the two-beam BIM, the two-beam SSM, and the 2-by-2 BS-MIMO systems, based on the measured channel matrix shown in Fig. 13, when the LoS link $h_{77}^{(b)}$ is available. The beam pairs (*i*, *j*) for the BIM and the transmit and receive beam indices for the SSM and the BS-MIMO are labelled in the legends.

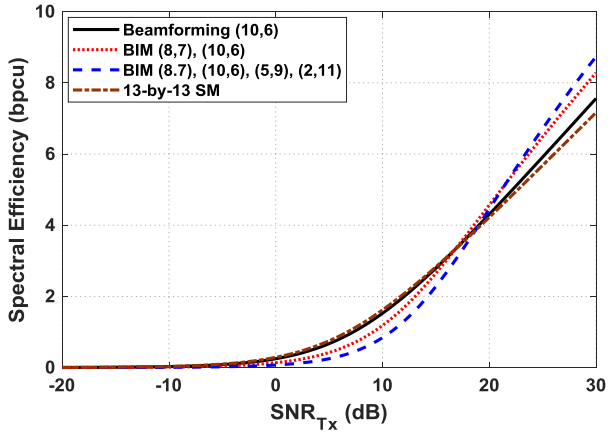

Fig. 16. Calculated spectral efficiencies of the beamforming, the 13-by-13 SM, and the BIM systems, based on the measured channel matrix shown in Fig. 13, when the LoS link $h_{77}^{(b)}$ is not available (we artificially assigned –70 dB to $\left|h_{77}^{(b)}\right|$). Two or four beam pairs, respectively, are selected for the BIM systems with transmit and receive beam index pairs (*i*, *j*) labelled in the legends.

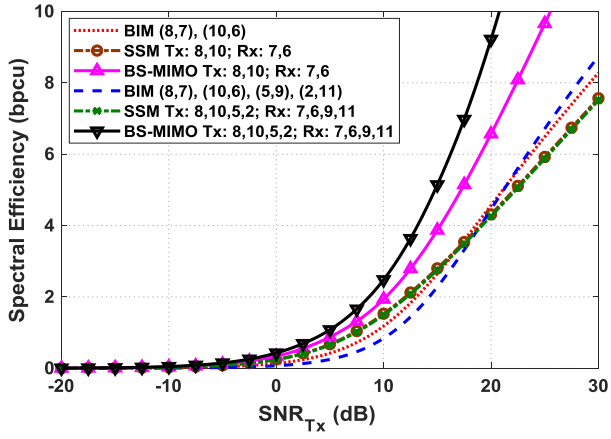

Fig. 17. Calculated spectral efficiencies of the BIM, the SSM, and the BS-MIMO systems, based on the measured channel matrix shown in Fig. 13, when the LoS link $h_{77}^{(b)}$ is not available (we artificially assigned –70 dB to $\left|h_{77}^{(b)}\right|$). The beam pairs (*i*, *j*) for the BIM and the transmit and receive beam indices for the SSM and the BS-MIMO are labelled in the legends.

addition, when the path gains of the selected beam pairs are more balanced, seen in Table I, greater number of beam pairs helps boost the performance within the high SNR region. This is because in the high SNR region the increase of SE_{BIM1}, e.g., from 0.93 to 1.79 *bpcu* when SNR_{Tx} is 30 dB, is more than enough to compensate the SE_{BIM2} loss, e.g., from 7.35 to 6.95 *bpcu* when SNR_{Tx} is 30 dB, if four beam pairs are used, instead of two. When comparing the BIM with the SSM and the BS-MIMO, see Fig. 17, the same observation can be obtained as we found out in Section IV, which is that the BS-MIMO systems with multiplexing capability have the superior performance, while the low beam crosstalk (or the sparsity of the channel) makes the SSM scheme, though equipping more receive RF chains, the worst choice.

Next, in order to confirm the limitation of the proposed BIM system, i.e., it underperforms the corresponding SM system in multipath-rich environments, another beam-space channel measurement was conducted in a different indoor lab environment, where more scatterers were present. The boresight of the transmit and the receive arrays was not aligned, and the LoS link was blocked, creating a great number of multipath links. The power of each entry of the measured 13-by-13 beam-space channel matrix is plotted in Fig. 18.

Two-beam and four-beam BIM systems are constructed using the beam-space channel matrix shown in Table II, and their spectral efficiencies, together with those of the beamforming and the 13-by-13 SM systems, are calculated and plotted in Fig. 19. It can be seen that while the two-beam BIM outperforms the beamforming in high SNR region, the four-beam BIM system has the worst performance, as the beam crosstalks are as high as $\left|h_{ij}^{(b)}\right|_{i=1,\,j=9} - \left|h_{ij}^{(b)}\right|_{i=1,\,j=10}$ = –1.4 dB, instead of –17.3 dB in the two-beam BIM system. In addition, the high beam crosstalk indicates the richness of the multipath links, making the 13-by-13 SM the best performed single-RF -chain transmission scheme.

When more RF chains are available at the receive sides, the SSM system can be constructed. As we concluded in Section IV, the low beam crosstalk level makes the two-beam BIM a better choice over the two-beam SSM in high SNR region, while the four-beam SSM could utilize more RF chains to harvest a greater amount of signal energy, compared with the single RF chain BIM system, when the high level of beam crosstalk exists, see Fig. 20. However, in this multipath-rich propagation environment, none of the BIM and the SSM could outperform the single-RF-chain SM scheme.

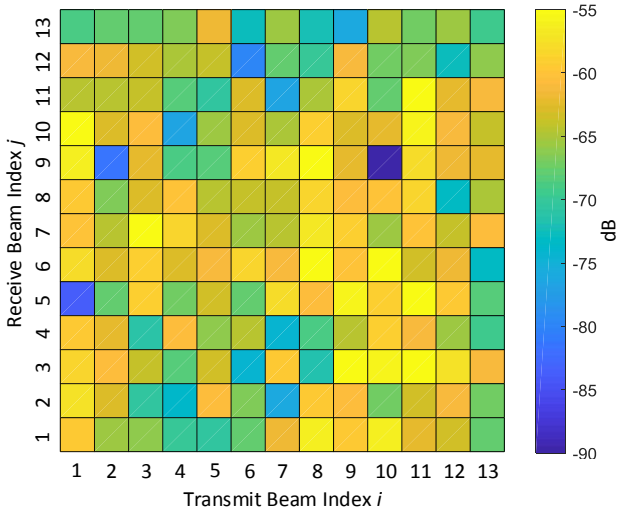

Fig. 18. Measured beam-space $\left|h_{ij}^{(b)}\right|$ in dB, at 10 GHz, when two identical communication nodes, each equipped with a 13-by-13 Fourier Rotman lens and a linear 13-element patch array, were placed in an indoor multipath-rich environment.

TABLE II

SELECTED BEAM-SPACE $\left|h_{ij}^{(b)}\right|$ IN DB, EXTRACTED FROM THE MEASURED CHANNEL MATRIX IN FIG. 18, FOR THE CONSTRUCTION OF TWO-BEAM (SHADED MATRIX) AND FOUR-BEAM BIM SYSTEMS.

$20\cdot\log_{10}\left\|h_{ij}^{(b)}\right\|$ (dB)		i = 1	3	10	8
j	10	–55.3	–60.8	–62.5	–59.0
	7	–60.3	–55.1	–65.7	–57.2
	3	–58.6	–63.9	–55.4	–72.0
	9	–56.7	–62.5	–94.3	–54.7

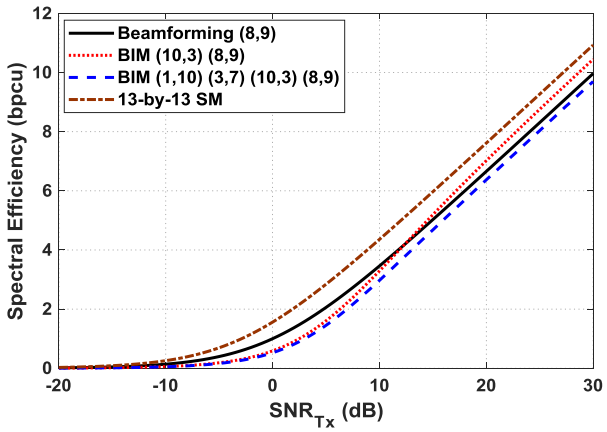

Fig. 19. Calculated spectral efficiencies of the beamforming, the 13-by-13 SM, and the BIM systems, based on the measured channel matrix shown in Fig. 18 and Table II. Two or four beam pairs, respectively, are selected for the BIM systems with transmit and receive beam index pairs (i, j) labelled in the legends.

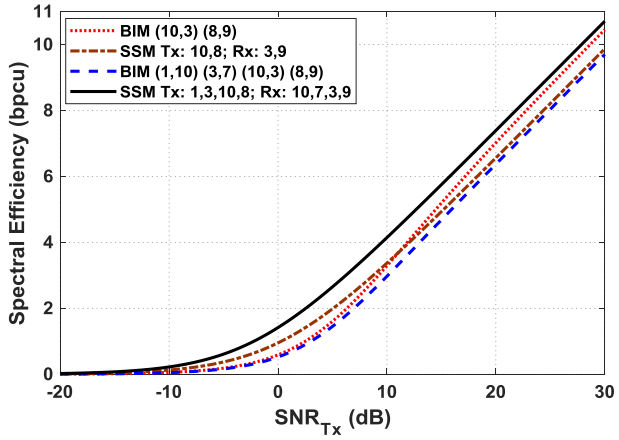

Fig. 20. Calculated spectral efficiencies of the two-beam and four-beam BIM systems, as well as their two-beam and four-beam SSM counterparts, based on the measured beam-space channel matrix shown in Fig. 18 and Table II. The beam pairs (i, j) for the BIM and the transmit and receive beam indices for the SSM are labelled in the legends.

VI. Conclusion

This paper extends the SM concept to the beam domain. In this way, we can construct BIM systems, which are attractive since each communication node in the BIM system requires only one RF chain. Through extensive simulations, it was shown that BIM systems can outperform the conventional beamforming and SM systems with commensurate hardware complexity in high SNR and nLoS high frequency sparse propagation channels. The BIM performance, compared with other various transmission schemes, and the associated general rules for beam pair selections have been further investigated using the measured beam-space channel matrices in some typical indoor multipath environments at 10 GHz. Further channel measurements at the mmWave frequency have been planned to study if the mmWave sparse channels could satisfy the channel conditions under which the proposed BIM is a favorable choice. Multi-user BIM scheme is also our future interest.

Appendix

In this Appendix, we derive the closed-form equation for the probability matrix $\boldsymbol{P}$ when two orthogonal beam pairs are available, i.e., $M = 2$ and $h_{12}^{(b)} = h_{21}^{(b)} = 0$.

At the transmitter side, when a complex Gaussian signal with power P_{Tx} is projected through the i^{th} ($i = 1$ or 2) transmit beam, the received signals at the i^{th} and j^{th} ($j \neq i$) receive beam ports, denoted as v_{ii} and v_{ij}, are independent and follow $CN(0, |h_{ii}|^2 P_{Tx}+\sigma^2)$ and $CN(0, \sigma^2)$, respectively. Since only power detection is performed, the resultant two power terms $|v_{ii}|^2$ and $|v_{ij}|^2$ follow the generalized Chi-squared distributions with their respective probability density functions given as

$$f(x) = \frac{1}{\left|h_{ii}^{(b)}\right|^2 P_{Tx} + \sigma^2} e^{\frac{-x}{\left|h_{ii}^{(b)}\right|^2 P_{Tx}+\sigma^2}}, \quad (x > 0) \tag{A1}$$

and

$$f(y) = \frac{1}{\sigma^2} e^{\frac{-y}{\sigma^2}}. \quad (y > 0) \tag{A2}$$

Thus, from (7),

$$\begin{aligned} p_{ii} &= p\left(|v_{ii}|^2 > |v_{ij}|^2\right) = \int_y^\infty \int_0^\infty f(x) f(y)\, dxdy \\ &= \int_0^\infty \frac{1}{\sigma^2} e^{\frac{-y}{\sigma^2}} \cdot e^{\frac{-y}{\left|h_{ii}^{(b)}\right|^2 P_{Tx}+\sigma^2}} dy \\ &= \frac{\left|h_{ii}^{(b)}\right|^2 P_{Tx} + \sigma^2}{\left|h_{ii}^{(b)}\right|^2 P_{Tx} + 2\sigma^2} = \frac{\left|h_{ii}^{(b)}\right|^2 SNR_{Tx} + 1}{\left|h_{ii}^{(b)}\right|^2 SNR_{Tx} + 2} \end{aligned}. \tag{A3}$$

With the calculated p_{11} and p_{22} in (A3), p_{12} and p_{21} can be easily obtained, since $p_{11} + p_{12} = 1$, and $p_{21} + p_{22} = 1$.

Acknowledgment

The authors thank Mr. Kieran Rainey for the help on the channel measurements. The authors also thank Taconic to provide Taconic RF-60A substrate for the Fourier Rotman lens fabrication.

References

[1] I. E. Telatar, "Capacity of multi-antenna Gaussian channels," *Eur. Trans. Telecommun.*, vol. 10, no. 6, pp. 585–595, Nov./Dec. 1999.

[2] R. Mesleh, H. Haas, S. Sinanovic, C. Ahn, and S. Yun, "Spatial modulation," *IEEE Trans. Veh. Technol.*, vol. 57, no. 4, pp. 2228–2241, Jul. 2008.

[3] P. Yang, M. Renzo, Y. Xiao, S. Li, and L. Hanzo, "Design guidelines for spatial modulation," *IEEE Commun. Surveys & Tutorials*, vol. 17, no. 1, pp. 6–26, First quarter 2015.

[4] E. Basar, M. Wen, R. Mesleh, M. Di Renzo, Y. Xiao, and H. Haas, "Index modulation techniques for next-generation wireless networks," *IEEE Access*, vol. 5, pp. 16693-16746, Sep. 2017.

[5] A. Stavridis, S. Sinanovic, M. Renzo, and H. Haas, "Energy evaluation of spatial modulation at a multi-antenna base station," in *Proc. IEEE 78th Veh. Technol. Conf. (VTC Fall)*, Las Vegas, NV, US, Sep. 2013, pp. 1–5.

[6] M. D. Renzo, H. Haas, A. Ghrayeb, S. Sugiura, and L. Hanzo, "Spatial modulation for generalized MIMO: challenges, opportunities, and implementation," *IEEE Proc.*, vol. 102, no., 1, pp. 56–103, Jan. 2014.

[7] A.Younis, N. Serafimovski, R. Mesleh, and H. Haas, "Generalised spatial modulation," in *Proc. Conf. Rec. 44th Asilomar Conf. Signals, Syst. Comput.*, Pacific Grove, CA, USA, Nov. 2010, pp. 1498–1502.

[8] J. Fu, C. Hou, W. Xiang, L. Yan, and Y. Hou, "Generalised spatial modulation with multiple active transmit antennas," in *Proc. IEEE Globecom Workshops*, Miami, FL, USA, Dec. 2010, pp. 839–844.

[9] N. Ishikawa, R. Rajashekar, S. Sugiura, and L. Hanzo, "Generalized-spatial-modulation-based reduced-RF-chain millimeter-wave communications," *IEEE Trans. Veh. Technol.*, vol. 66, no. 1, pp. 879–883, Jan. 2017.

[10] J. Wang, S. Jia, and J. Song, "Generalised spatial modulation system with multiple active transmit antennas and low complexity detection scheme," *IEEE Trans.Wireless Commun.*, vol. 11, no. 4, pp. 1605–1615, Apr. 2012.

[11] K. Ntontin, M. Di Renzo, A. Perez-Neira, and C. Verikoukis, "Performance analysis of multistream spatial modulation with maximum-likelihood detection," in *Proc. IEEE Global Commun. Conf. (GLOBECOM)*, Atlanta, GA, USA, Dec. 2013, pp. 1590–1594.

[12] A. Ibrahim, T. Kim, and D. Love, "On the achievable rate of generalized spatial modulation using multiplexing under a gaussian mixture model," *IEEE Trans. Commun.*, vol. 64, no. 4, pp. 1588–1599, Apr. 2016.

[13] R. Mesleh, S. Ikki, and H. Aggoune, "Quadrature spatial modulation," *IEEE Trans. Veh. Technol.*, vol. 64, no. 6, pp. 2738–2742, Jun. 2015.

[14] Z. Yigit and E. Basar, "Low-complexity detection of quadrature spatial modulation," *Electron. Lett.*, vol. 52, no. 20, pp. 1729–1731, Sep. 2016.

[15] C. Cheng, H. Sari, S. Sezginer, and Y. T. Su, "Enhanced spatial modulation with multiple signal constellations," *IEEE Trans. Commun.*, vol. 63, no. 6, pp. 2237–2248, Jun. 2015.

[16] P. Liu, M. Renzo, and A. Springer, "Line-of-sight spatial modulation for indoor mmWave communication at 60 GHz," *IEEE Trans. Wireless Commun.*, vol. 15, no. 11, pp. 7373–7389, Nov. 2016.

[17] P. Liu, M. Renzo, and A. Springer, "Variable-N_u generalized spatial modulation for indoor LOS mmWave communication: performance optimization and novel switching structure," *IEEE Trans. Commun.*, vol. 65, no. 6, pp. 2625–2640, Jun. 2017.

[18] P. Liu, J. Blumenstein, N. S. Perovic, M. Di Renzo, and A. Springer, "Experimental assessment of generalized spatial modulation MIMO over60 GHz indoor channels," *IEEE Trans. Commun.*, to be published.

[19] I. Sarris and A. Nix, "Design and performance assessment of high capacity MIMO architectures in the presence of a line-of-sight component," *IEEE Trans. Veh. Tech.*, vol. 56, no. 4, pp. 2194–2202, Jul. 2007.

[20] Z. Li, L. Zhou, A. Honda, and Y. Ohashi, "Spatial multiplexing of 4×4 UCA LoS MIMO systems with splitting matrix at RF band," in *Proc. 9th Eur. Conf. Antennas propag. (EuCAP)*, Lisbon, Portugal, Apr. 13–17, 2015, pp. 1–4.

[21] A. Maltsev *et al*., *Channel Models for 60 GHz WLAN Systems*, IEEE Standard 802.11-09/0334r8, May 2010. https://mentor.ieee.org/802.11/dcn/09/11-09-0334-08-00ad-channel-models-for-60-GHz-WLAN-systems.doc

[22] E. Torkildson, B. Ananthasubramaniam, U. Madhow, and M. Rodwell, "Millimeter-wave MIMO: wireless links at optical speeds," in *Proc. 44th Allerton Conf. Commun., Control Compu.*, Sep. 2006.
[23] Z. Li, S. Han, and A. Molisch, "Hybrid beamforming design for millimeter-wave multi-user massive MIMO downlink," in *Proc. IEEE Int. Conf. Commun. (ICC)*, Kuala Lumpur, Malaysia, May 22–27, 2016, pp. 1–6.
[24] A. Molisch *et al*., "Hybrid beamforming for massive MIMO: a survey," *IEEE Commun. Mag.*, vol. 55, no. 9, pp. 134–141, Sep. 2017.
[25] Y. Ding and V. Fusco, "Sidelobe manipulation using Butler matrix for 60 GHz physical layer secure wireless communication," in *Proc. Antennas Propag. Conf.*, Loughborough, U.K., Nov. 11–12, 2013, pp. 61–65.
[26] Y. Zhang, Y. Ding, and V. Fusco, "Sidelobe modulation scrambling transmitter using Fourier Rotman lens," *IEEE Trans. Antennas Propag.*, vol. 61, no. 7, pp. 3900–3904, Jul. 2013.
[27] Y. Ding, K. Kim, T. Koike-Akino, M. Pajovic, P. Wang, and P. Orlik, "Spatial scattering modulation for uplink millimeter-wave systems," *IEEE Commun. Lett.*, vol. 21, no. 7, pp. 1493–14964, Jul. 2017.
[28] F. Dai and J. Wu, "Efficient broadcasting in Ad Hoc wireless networks using directional antennas," *IEEE Trans. Parallel Dist. Sys.*, vol. 17, no. 4, pp. 335–347, Apr. 2006.
[29] J. Wang, Z. Lan, C. W. Pyo, T. Baykas, C. S. Sum, M. Azizur Rahman, R. Funada, F. Kojima, I. Lakkis, H. Harada, and S. Kato, "Beam codebook based beamforming protocol for multi-Gbps millimeter-wave WPAN systems," *IEEE J. Sel. A. Commun.*, vol. 27, no. 8, pp. 1390–1399, Oct. 2009.
[30] Y. Tsang, A. Poon, and S. Addepalli, "Coding the beams: improving beamforming training in mmWave communication system," in *IEEE Global Telecommun. Conf.* (*GLOBECOM 2011*), Houston, TX, USA, Dec. 5–9, 2011, pp. 1–6.
[31] HMC1094 data sheet, [Online]. Available: http://www.analog.com/media/en/technical-documentation/data-sheets/HMC1094.pdf
[32] N. S. Perović, P. Liu, M. D. Renzo, and A. Springer, "Receive spatial modulation for LOS mmWave communications based on TX beamforming," *IEEE Commun. Lett.*, vol. 21, no. 4, pp. 921–924, Apr. 2017.
[33] J. Jeganathan, A. Ghrayeb, and L. Szczecinski, "Spatial modulation: optimal detection and performance analysis," *IEEE Commun. Lett.*, vol. 12, no. 8, pp. 545–547, Aug. 2008.
[34] R. C. Daniels, J. N. Murdock, T. S. Rappaport, and R. W. Heath, Jr., "60 GHz wireless: up close and personal," *IEEE Microw. Mag.*, vol. 11, no. 7, pp. 44–50, Dec. 2010.
[35] J. Brady, N. Behdad, and A. Sayeed, "Beamspace MIMO for millimeter-wave communications: system architecture, modeling, analysis, and measurements," *IEEE Trans. Antennas Propag.*, vol. 61, no. 7, pp. 3814–3827, Jul. 2013.
[36] P. Amadori and C. Masouros, "Low RF-complexity millimeter-wave beamspace-MIMO systems by beam selection," *IEEE Trans. Commun.*, vol. 63, no. 6, pp. 2212–2223, Jun. 2015.
[37] M. Molu, P. Xiao, M. Khalily, K. Cumanan, L. Zhang, and R. Tafazolli, "Low-complexity and robust hybrid beamforming design for multi-antenna communication systems," *IEEE Trans.Wireless Commun.*, to be published.
[38] R. Lai, S. Chao, Z. Tsai, J. Lee, and H. Wang, "Topology analysis and design of passive HEMT millimeter-wave multiple-port switches," *IEEE Trans. Microw. Theory Tech.*, vol. 56, no. 7, pp. 1545–1554, Jul. 2008.
[39] M. Liu, R. Jin, J. Geng, and X. Liang, "Low-insertion loss pin diode switches using impedance-transformation networks," *Progr. Electromagn. Res. C*, vol. 34, pp. 195–202, 2013.
[40] D. Bliss, K. Forsythe, and A. Chan, "MIMO wireless communication," *Lincoln Laboratory J.*, vol. 15, no. 1, pp. 97–126, 2005.
[41] Y. Yang and B. Jiao, "Information-guided channel hopping for high data rate wireless communication," *IEEE Commun. Lett.*, vol. 12, no. 4, pp. 225–227, Apr. 2008.
[42] R. Rajashekar, K. Hari, and L. Hanzo, "Reduced complexity ML detection and capacity-optimized training for spatial modulation systems," *IEEE Trans. Commun.*, vol. 62, no. 1, pp. 112–125, Jan. 2014.
[43] P. Henarejos and A. I. Pérez-Neira, "Capacity analysis of index modulations over spatial, polarization, and frequency dimensions," *IEEE Trans. Commun.*, vol. 65, no. 12, pp. 5280–5292, Dec. 2017.
[44] P. McIllree, "Channel capacity calculations for M-Ary N-dimensional signal sets," M.E. thesis in Electronic Engineering, Univ. of South Australia, Adelaide, Australia, 1995.
[45] K. Du and M. Swamy, *Wireless Communication Systems: From RF Subsystems to 4G Enabling Technologies*. Cambridge, U.K.: Cambridge Univ. Press, 2010, pp. 571–575.
[46] Y. Ding, Y. Zhang, and V. Fusco, "Fourier Rotman lens enabled directional modulation transmitter," *Int. J. Antennas Propag.*, vol. 2015, pp. 1–13, 2015.

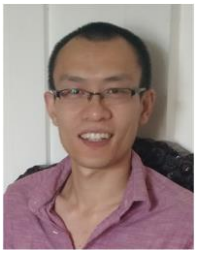

Yuan Ding received his Bachelor's degree from Beihang University (BUAA), Beijing, China, in 2004, received his Master's degree from Tsinghua University, Beijing, China, in 2007, and received his Ph.D. degree from Queen's University of Belfast, Belfast, UK, in 2014, all in Electronic Engineering.

He was a radio frequency (RF) Engineer in Motorola R&D Centre (Beijing, China) from 2007 to 2009, before joining Freescale Semiconductor Inc. (Beijing, China) as an RF Field Application Engineer, responsible for high power base-station amplifier design, from 2009 to 2011. He is now an Assistant Professor at the Institute of Sensors, Signals and Systems (ISSS) in Heriot-Watt University, Edinburgh, UK. His research interests are in antenna array, physical layer security, and 5G related areas.

Dr. Ding was the recipient of the IET Best Student Paper Award at LAPC 2013 and the recipient of the Young Scientists Awards in General Assembly and Scientific Symposium (GASS), 2014 XXXIst URSI.

Vincent F. Fusco (S'82–M82–SM'96– F'04) received the bachelor's (Hons.) degree in electrical and electronic engineering, the Ph.D. degree in microwave electronics, and the D.Sc. degree from Queen's University Belfast (QUB), Belfast, U.K., in 1979, 1982, and 2000, respectively.

His work was focused on advanced front-end architectures with enhanced functionality. He is Chief Technology Officer (CTO) of the ECIT at QUB. He has authored over 450 scientific papers in major journals and in referred international conferences. He has authored two textbooks, holds patents related to self-tracking antennas, and has contributed invited papers and book chapters. His current research interests include active antenna and front-end MMIC techniques.

Prof. Fusco is a fellow of the Institute of Electrical and Electronics Engineers, the Institution of Engineering and Technology, the Royal Academy of Engineers, and the Royal Irish Academy. In 2012, he received the IET Senior Achievement Award and the Mountbatten Medal. He serves on the Technical Program Committee of various international conferences, including the European Microwave Conference.

Alexey P. Shitvov (M'06) received Diploma Engineer degree in semiconductor devices and microelectronics from the Nizhny Novgorod State University (NNSU), Nizhny Novgorod, Russia, in 1995, and a Ph.D. degree in Electronics and Electrical Engineering from the Queen's University Belfast (QUB), Belfast, U.K. in 2009.

From 2009 to 2014 he was a Royal Academy of Engineering Research Fellow with the ECIT Institute, QUB, conducting research on phenomenology and mitigation of passive intermodulation in communication components and systems. He was a Lecturer in the millimeter-wave and sub-millimeter wave passive and active components and devices with the School of Electronics, Electrical Engineering and Computer Science, QUB, from 2013 to 2017. He is currently a Research Associate with the Astronomy Instrumentation Group, School of Physics and Astronomy, Cardiff University, U.K., working on the theory and application of graded metasurfaces at millimeter-wave frequencies. His research interests include characterization and modelling of nonlinearities in communication systems, advanced microwave materials, millimeter-wave communication and sensing system design under hardware constraints, and electromagnetic metasurfaces for arbitrary phase, polarization and wave-front control.

Yue Xiao received the Ph.D degree in communication and information systems from the University of Electronic Science and Technology of China (UESTC) in 2007. He is currently a Professor with National Key Laboratory of Science and Technology on Communications, UESTC. He has published more than 100 international journal papers and has been in charge of more than 20 projects in the area of Chinese 3G/4G/5G wireless communication systems. He is an inventor of more than 50 Chinese and PCT patents on wireless systems. His research interests are in system design and signal processing toward future wireless communication systems. He currently serves as an Associate Editor of IEEE COMMUNICATIONS LETTERS.

Hailin Li received his Ph.D. degree in signal and information processing from the Nanjing University of Aeronautics and Astronautics (NUAA), Nanjing, China, in 2013. He is a lecturer in the College of Electronic and Information Engineering of NUAA. His research interests include image processing, digital signal processors, and array signal processing.